Size-dependent phase transition of Er_2O_3 under high pressure

Xiangting Ren, Xiaozhi Yan, Zhenhai Yu, Wentao Li, Ke Yang, Xiaoli Wang, Yuzi Liu, and Lin Wang

Citation: Appl. Phys. Lett. **112**, 143102 (2018); doi: 10.1063/1.5017815
View online: https://doi.org/10.1063/1.5017815
View Table of Contents: http://aip.scitation.org/toc/apl/112/14
Published by the American Institute of Physics

Size-dependent phase transition of Er_2O_3 under high pressure

Xiangting Ren,[1] Xiaozhi Yan,[1] Zhenhai Yu,[1] Wentao Li,[1,2] Ke Yang,[3] Xiaoli Wang,[4,a)] Yuzi Liu,[5,a)] and Lin Wang[1,a)]

[1]*Center for High Pressure Science and Technology Advanced Research (HPSTAR), Shanghai 201203, China*
[2]*Institute of Atomic and Molecular Physics, Sichuan University, Chengdu 610065, China*
[3]*Shanghai Synchrotron Radiation Facility (SSRF), Shanghai Institute of Applied Physics, Chinese Academy of Science, Shanghai 201800, China*
[4]*School of Physics and Electronic Engineering, Linyi University, Linyi 276005, China*
[5]*Center for Nanoscale Materials, Argonne National Laboratory, 9700 South Cass Avenue, Argonne, Illinois 60439, USA*

(Received 30 November 2017; accepted 25 February 2018; published online 2 April 2018)

The size effect on the structural and optical properties of cubic Er_2O_3 was investigated under pressure by *in-situ* angular dispersive synchrotron x-ray diffraction (AD-XRD), Raman scattering, photoluminescence (PL), and impedance spectroscopy. Contrary to the phase transition sequence of cubic→monoclinic→hexagonal in bulk Er_2O_3, a transformation from cubic directly to hexagonal was observed in Er_2O_3 nanoparticals. Compared with bulk Er_2O_3, nano-Er_2O_3 showed an obvious elevation of phase transition pressure and larger bulk module. A third-order Birch-Murnaghan fitting yields zero pressure bulk moduli (B_0) of 181(5), and 226(4) GPa and their pressure derivatives (B'_0) of 4.0(7), 1.9(5) for the cubic and hexagonal phases, respectively. The multiple PL lines of $^4S_{3/2}\rightarrow{}^4I_{15/2}$ originating from the cubic phase are also altered due to phase transformation. The impedance spectroscopy indicated that the nano-Er_2O_3 is an insulator up to 30 GPa. These findings give a fresh understanding of size influence on the phase transition sequences and sheds light on the applications of nano-Er_2O_3. *Published by AIP Publishing.* https://doi.org/10.1063/1.5017815

Size effects at the nanoscale (less than 100 nm) have significant consequences on the structural and physical properties of materials, and have received a considerable interest to investigate behavior of nanosized materials at high pressure. For instance, the yield strength of nano-Ni measured under triaxial compression is significantly higher than bulk Ni.[1] A remarkable strength weakening was evidenced in ~10 nm anatase TiO_2 comparing to their bulk counterparts.[2] The compressibility and the transition pressure in CdSe,[3] Si,[4] and ZnO[5] are significantly elevated with the decrease in crystal size, especially in nanoscale, which has been explained by a higher surface energy of the nanoscale materials compared to the bulk materials. Conversely, γ-Fe_2O_3[6] and CeO_2[7] display a lower phase transition pressure with a decrease in crystal size, which is explained by a large volume collapse. Size effects on the high-pressure phonon spectra of nano anatase TiO_2 showed differences to bulk materials in the slopes of Raman modes shifts with pressure.[8] Compared with the initial red-shift and then blue shift of the PL spectra in bulk $CsPbBr_3$, the blue-shift of the PL spectra in the $CsPbBr_3$ nanocubes was not observed under high pressure.[9] All of these results demonstrate distinct properties of nanomaterials at high pressure owing to the size effects.

Erbium sesquioxides (Er_2O_3), which is a well known rare-earth sesquioxides (Re_2O_3), a family that exhibits various polymorphs and unique physicochemical properties, has been widely used in laser and optical amplifiers.[10,11] These applications are strongly structural dependent, and the size effect plays a critical role in enhancing the physicochemical properties of Er_2O_3.[12] The cubic→monoclinic→hexagonal phase transition sequence was usually expected in bulk Re_2O_3[13–15] by applying high pressure. The effect of pressure on Er_2O_3 has been previously investigated both by experiments and theoretical calculations.[16–22] A monoclinic Er_2O_3 (B-type, space group $C2/m$) was synthesized in a large volume at 3 GPa and 1020 °C.[21] Guo *et al.*[17] observed a cubic (C-type, space group Ia-3) to monoclinic phase transition at 9.9 GPa in submicron Er_2O_3 by energy-dispersive XRD. Theoretical calculations predicted a phase transition from monoclinic to hexagonal (A-type, space group P-3m1) at 22 GPa[19] and 19.4 GPa.[18] Successive phase transition of C→B→A and C→B were found in submicron Er_2O_3[22] and nano Er_2O_3 with the grain size of 20 nm,[18] respectively. Also, the direct transition from C to A has been found in many Re_2O_3 nanocrystals, such as Y_2O_3[23] and Dy_2O_3.[24] This motivated us to reexamine the size effect on the structural transition and properties of nano-Er_2O_3.

In this study, we investigated the influence of size effect on the phase transition of Er_2O_3 by using synchrotron x-ray diffraction, Raman scattering, and PL spectrum. The C→A instead of C→B→A transition was observed in nano-Er_2O_3. The bulk moduli of the C- and A-type nano-Er_2O_3 were obtained. Our results demonstrate that the stability and transition routines of Er_2O_3 are grain size dependent.

Nanosized Er_2O_3 with a purity of 99.9% was used as the starting material. An Er_2O_3 thin slice with a ruby ball was loaded into a gasketed diamond anvil cell (DAC). The pressure was determined by the shift of R1 fluorescence line of ruby.[25] Silicone oil was used as the pressure transmitting medium (PTM) in the XRD, Raman scattering, and PL spectra measurements. The *in situ* high-pressure XRD experiments were performed at the BL15U1 station of the Shanghai

a)Authors to whom correspondence should be addressed: wanglin@hpstar.ac.cn; yuziliu@anl.gov; and wxl@lyu.edu.cn

Synchrotron Radiation facility (SSRF) with a wavelength of 0.6199 Å.[26] The collected 2D diffraction patterns were integrated into one-dimensional spectra using FIT2D software.[27] The Raman spectra were measured with a 473 nm excitation laser with Princeton Instruments Acton Series. The PL spectra were collected by using a Renishaw inVia Raman system with a 532 nm laser. A two-electrode (Pt electrodes) configuration was used for *in-situ* electrical impedance spectroscopy measurement. No PTM was used for this measurement. The impedance spectra were measured by a Solartron 1260 impedance analyzer equipped with Solartron 1296 dielectric interface. A 5 V sine signal was applied to the sample, and its frequency ranged from 3×10^{-2} to 4×10^{6} Hz.

The crystal structure and grain size of the sample were analyzed using XRD and TEM, as shown in Fig. 1. Figure 1(a) is a typical GSAS[28] refinement of the XRD pattern of the nano-Er_2O_3 at ambient condition and the inset shows its schematic crystal structure. The powder XRD data of nano-Er_2O_3 can be indexed to a cubic structure with space group *Ia*-3 (No. 206) with the lattice parameter a = 10.5493 Å, 16 molecules per unit cell, and six-fold coordinated Er^{3+}. The TEM image [Fig. 1(b)] and the corresponding grain size distribution [Fig. 1(c)] show that the size of the nano-Er_2O_3 is mainly 19 ± 5 nm.

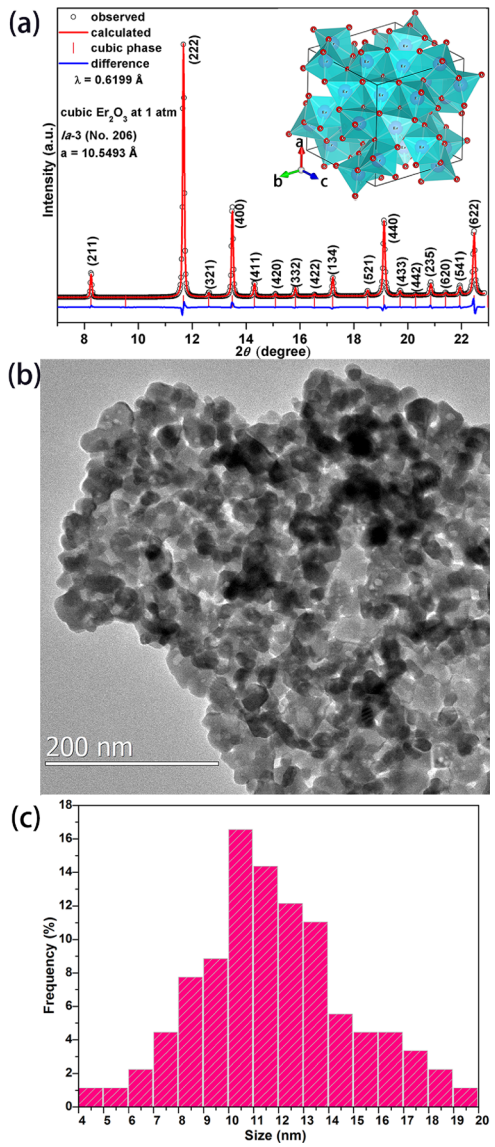

FIG. 1. (a) Refinement of the XRD pattern of nanosized Er_2O_3 at ambient conditions. The inset shows the schematic crystal structure of cubic Er_2O_3. (b) TEM image and (c) its correspondent grain size distribution of nano-Er_2O_3 at ambient conditions.

We conducted quasi-hydrostatic compression measurements to elucidate the size effect on the high-pressure behavior of Er_2O_3 in silicon oil. Figure 2(a) shows the integrated patterns at selected pressures. As portrayed in Fig. 2(a), the diffraction peaks of the C-type phase shifted to higher angles with the contraction of the unit cell. No structure change was observed up to 15.1 GPa apart from the shift and broaden of the peaks. When the pressure reached 17 GPa, a new weak peak belonging to A-type phase emerged. With pressure increasing, the peaks from the C-type gradually disappeared and the peaks from the A-type increasing. It was found that C- ($a = 10.14252$ Å) and A-type ($a = 3.54825$ Å, $c = 5.51576$ Å) phases coexist at 24.3 GPa by XRD pattern Rietveld refinement shown in Fig. 2(b). When the applied pressure is over 30 GPa, only A-type was remained up to the highest pressure applied. Following the pressure release, the A-type transformed to B-type, which was quenchable at ambient conditions. Our results showed that the size dependent phase transition sequence of nano-Er_2O_3 is C→A instead of C→B[17] or C→B→A[22] in compression, and the phase transition sequence is A→B upon pressure release. The comparison of the onset transition pressure with bulk materials was listed in Table I. The phase transition pressure of nano-Er_2O_3 (17 GPa) in this study is higher than the reported values. Such enhancement of structure stability in nano-Er_2O_3 might be induced by the higher surface energy such as ZnO[5] and SnO_2.[29]

Figure 2(c) shows pressure dependence of the lattice parameters of the C- and A-type nano-Er_2O_3 at room temperature. The axial compressibilities are characterized by kappa parameter κ ($\kappa = (L_0 - L_p)/P$, L_0 is the lattice parameter at ambient condition, L_p is the lattice parameter under high pressure P, and κ is in Å/GPa. We found the compressibilities along the c axis in the A-type phase and along the a axis in the C-type phase have the same order of magnitude. In contrast, the compressibility along the a axis in the A-type phase is about one order of magnitude smaller. The anisotropic axial compressibility of the A-type phase for nano-Er_2O_3 is in good agreement with other A-type Re_2O_3.[30–32] Figure 2(d) illustrates the pressure dependent volume of the C- and A-type phases for nano-Er_2O_3. The pressure-volume data could be fitted to a third-order Birch-Murnaghan equation of state (BM-EoS)[33–35]

$$P = 3/4B_0\left[(V_0/V)^{7/3} - (V_0/V)^{5/3}\right] \times \{1 + 3/4(B_0')\,[(V_0/V)^{2/3} - 1]\},$$

where B_0 and B'_0 are the bulk modulus and its pressure derivative, respectively. V_0 and V are the volume at ambient condition and pressure P, respectively.

The bulk modulus of the C- and A-type phases yield from the fitting are $B_0 = 181(5)$ GPa, $V_0 = 73.37(5)$ Å^3, $B'_0 = 4.0(7)$, and $B_0 = 226(4)$ GPa, $V_0 = 66.06(8)$ Å^3, $B'_0 = 1.9(5)$, respectively. The C→B and C→A phase transition are reconstructive

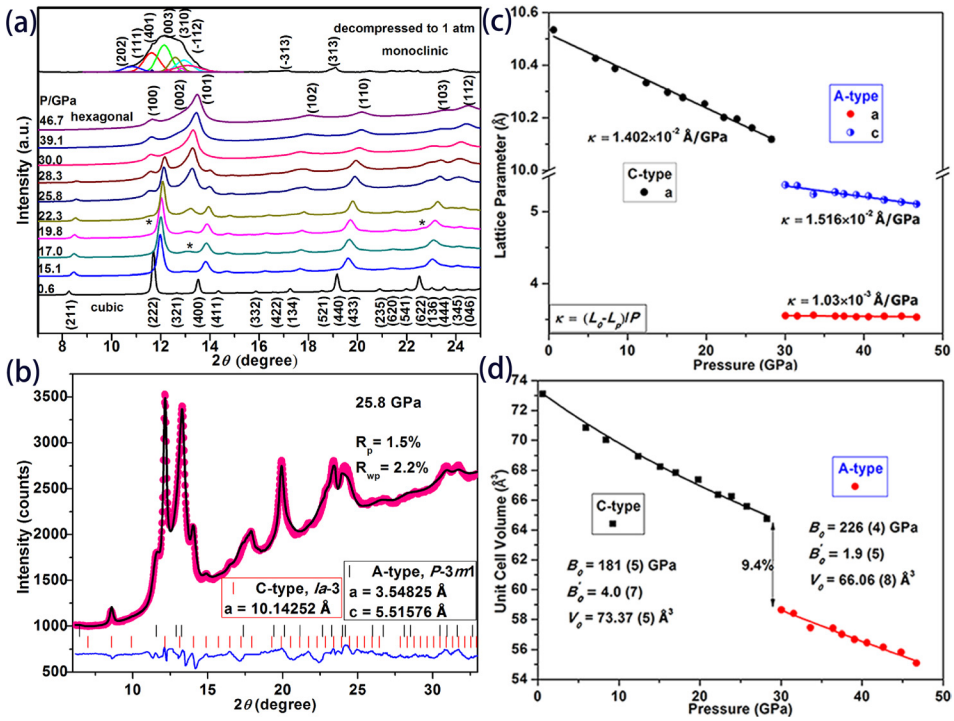

FIG. 2. (a) Selected high-pressure powder XRD patterns of nano-Er_2O_3 in silicon oil. (b) The GSAS refinement results of nano-Er_2O_3 at 25.8 GPa. The experimental and calculated data are represented by the black cross and red line. The difference between the observed and the fitted XRD patterns are shown with a blue line at the bottom. (c) Pressure-dependence of lattice parameters for C- and A-type nano-Er_2O_3 at room temperature. (d) Pressure dependent unit cell volume for C- and A-type nano-Er_2O_3.

TABLE I. Comparison of the onset phase transition pressure (P_{on}), the bulk modulus (B_0), and its pressure derivative (B'_0) of cubic Er_2O_3 in previous studies with silicon oil as the PTM.

Sample	P_{on} (GPa)	B_0 (GPa)	B'_0	References
Submicron	6.6	151.2	4 (fixed)	17
Submicron	9.9	200(6)	8.4	12
Nanoparticle	13.8	231(3)	4 (fixed)	15
		211(4)	8.4 (fixed)	
Nanoparticle	17	181(5)	4.07	This work

and the volume change should be large.[36] Guo *et al.* reported the C→B phase transition was accompanied by a 9% volume decrease in submicron Er_2O_3.[17] The C→A phase transition in nano-Er_2O_3 is accompanied by a 9.4% volume decrease. Compared with the previously reported data (with the same pressure medium, in Table I), we can see an obvious size effect on the stability and compressibility of Er_2O_3. The results indicated that the onset phase transition pressure (P_{on}) and the B_0 of C-type bulk-Er_2O_3 increase with the reduction of the crystal size. As seen in Table I, the B_0 of nano-Er_2O_3 is 181(5) GPa), which is ~20% larger than the B_0 of C-type bulk-Er_2O_3 (~151 GPa).[22] The B_0 achieved in this work is smaller than which reported in Refs. 12 and 15. It might be because of the quasi-hydrostatic pressure condition.[37]

The optical properties of materials are closely related to their electronic structure, which is determined by their crystal structure. To verify the proposed structural transition in nano-Er_2O_3, we performed high-pressure Raman scattering [Fig. 3(a)] and PL spectroscopy [Fig. 3(b)] measurement to identify the phase transition. Silicon oil was adopted as a PTM. Twenty-two Raman modes ($4A_g + 4E_g + 14F_g$) have been predicted for the C-type Er_2O_3 according to group theory analysis.[38] Due to the strong luminescence and absorption effects of Er_2O_3, only 6 Raman peaks for the cubic phase were observed in this study. The most prominent peak

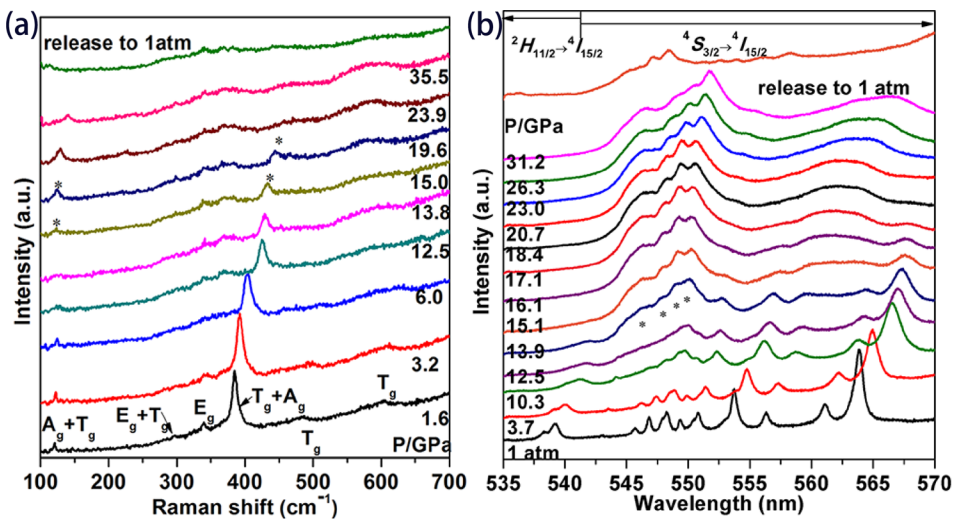

FIG. 3. (a) Raman spectra of nano-Er_2O_3 at selected pressures. (b) PL spectra of nano-Er_2O_3 at selected pressures.

assigned as the $T_g + A_g$ band occurs at $\sim 380\,cm^{-1}$ is the characteristic peaks of the C-type Er_2O_3. With pressure increasing, the intensity of all the Raman modes reduced and broadened. Only the $T_g + A_g$ band could be visible and continuously shift to higher wavenumbers, indicating the contraction of the lattice constants under high pressure. At 19.6 GPa, the change of the relative intensity of the two Raman peaks at $\sim 123\,cm^{-1}$ and $\sim 433\,cm^{-1}$ (labeled with an asterisk) implied the structural change occurred between 15.0 and 19.6 GPa. This transition is irreversible as seen from the Raman spectra of the sample quenched to room pressure. The observed pressure-induced phase transition in Raman spectra is in agreement with XRD observations.

Figure 3(b) showed the evolution of the PL spectra for nano-Er_2O_3. It is in good agreement with a previous study.[39] The luminescence peaks shifted to longer wavelength and lost intensity with increasing pressure. When the pressure reached 13.9 GPa, some new peaks (labeled as asterisk) attributed to the $^4S_{3/2} \rightarrow {}^4I_{15/2}$ transition appeared and became stronger while some original peaks weakened and disappeared, which suggested the onset of cubic-hexagonal phase transition. The PL peaks of the hexagonal phase were not preserved and transformed to the monoclinic structure after the pressure got released. The PL spectra evolution in nano-Er_2O_3 was in good agreement with our XRD results and further proved the phase transitions of Er_2O_3.

We investigated the transport properties of nano-Er_2O_3 by impedance spectroscopy measurements with pressure up to 30.4 GPa. Figure 4(a) displays the Nyquist plots of the impedance spectra of nano-Er_2O_3 at different pressures. Only one arc is observed in our experiments. It means that the grain conduction dominates the electrical transport properties of nano-Er_2O_3.[30] The impedance spectroscopy was modeled with an equivalent circuit. The grain resistance values as a function of pressure [in Fig. 4(b)] were obtained by fitting the data of the circuit parameters using ZView impedance analysis software.[40] The results showed an abrupt increase in grain resistance from 16.3 to 18.5 GPa and then turns around up to 30.4 GPa. The abnormal increase in grain resistance at 16.3 GPa is consistent with the C→A phase transition which was observed in XRD, Raman, and PL measurements. It should be attributed to the phase transition. The impedance spectroscopy measurements suggest the nano-Er_2O_3 is an insulator under the pressure up to 30 GPa.

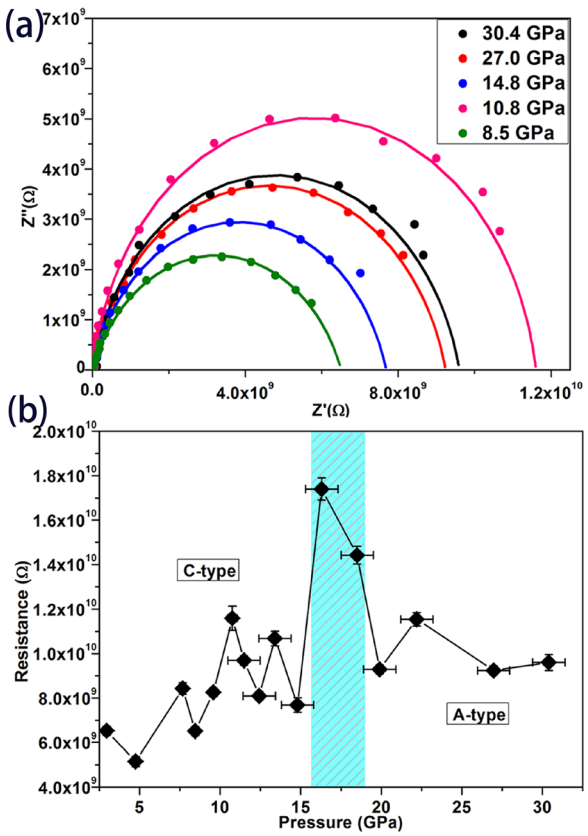

FIG. 4. High pressure alternating current impedance spectroscopy measurements. (a) Selected Nyquist diagram of nano-Er_2O_3 at various pressures. (b) The pressure dependence of the grain resistance.

Under compression at room temperature, the normal phase transition sequence of C→B→A[22] and C→B[17] was found in submicron Er_2O_3. The expected B-type Er_2O_3 was bypassed in this study, although the C→B phase transformation was reported in Ref. 20. The size-dependent phase transition sequence in Er_2O_3 is very similar with that observed in TiO_2,[41,42] Y_2O_3,[23] PbTe,[43] ZrO_2,[44] and Dy_2O_3.[24] For example, the same phase transition sequence of C→B→A was reported in bulk Dy_2O_3[13] and Y_2O_3.[45] The phase transition of C→A was suggested in a Raman scattering study of nano-Dy_2O_3.[24] In the case of Y_2O_3,[23] 21 nm-sized sample underwent a C→A phase transition while 16 nm-sized Y_2O_3 underwent a crystalline→amorphous transition. The underneath mechanism is known as the different surface energy between the high and low pressure phases which influences the thermodynamics of solid-solid phase transitions in nanocrystals. Also, the high surface energy of nanoparticles leads to enhanced transition pressure in most materials. It is reasonable that the free energy of A-type phase in nanoscale is lower than the B-type phase. Our study demonstrates that the high surface energy of nanomaterials can remarkably modify the phase transition sequences and phase stability of E_2O_3.

In conclusion, the irreversible high-pressure induced phase transition of nano-Er_2O_3 was investigated experimentally using XRD, Raman scattering, PL and impedance spectra techniques. The B_0 for the cubic phase of nano-Er_2O_3 is ~20% larger than its bulk counterpart. Our results showed that the decrease in crystal size not only increased the phase stability and compressibility but also changed the phase transition sequence of nano-Er_2O_3. It was found that that the PL properties of Er_2O_3 were altered with the structural phase transition. The abnormal increase in grain resistance at 16.3 GPa also confirmed the C→A phase transition. The impedance spectroscopy measurements suggest the nano-Er_2O_3 is an insulator up to 30 GPa.

We acknowledge the support of National Science Associated Funding (Grant No. U1530402), Science Challenging Program (Grant No. JCKY2016212A501), and National Natural Science Foundation of China (Grant No. 11704014). This work was also supported by the National Natural Science Foundation of China under Grants No. 11674144 and Natural Science Foundation of Shandong Province No. JQ201602. The X-ray diffraction and Raman scattering measurements were performed at the BL15U1

station, Shanghai Synchrotron Radiation Facility (SSRF) in China. The use of the Center for Nanoscale Materials and the Advanced Photon Source, both Office of Science user facilities, was supported by the U.S. Department of Energy, Office of Science, Office of Basic Energy Sciences, under Contract No. DE-AC02-06CH11357.

[1]Y. Zhao, J. Zhang, B. Clausen, T. D. Shen, G. T. Gray III, and L. Wang, Nano Lett. **7**, 426 (2007).
[2]Y. Wang, J. Zhang, and Y. Zhao, Nano Lett. **7**(10), 3196–3199 (2007).
[3]S. H. Tolbert, Science **265**, 373 (1994).
[4]S. H. Tolbert, A. B. Herhold, L. E. Brus, and A. P. Alivisatos, Phys. Rev. Lett. **76**, 4384 (1996).
[5]J. Jiang, J. Olsen, L. Gerward, D. Frost, D. Rubie, and J. Peyronneau, Europhys. Lett. **50**, 48 (2000).
[6]J. Jiang, J. S. Olsen, L. Gerward, and S. Mørup, Europhys. Lett. **44**, 620 (1998).
[7]Z. W. Wang, S. K. Saxena, V. Pischedda, H. P. Liermann, and C. S. Zha, Phys. Rev. B **64**, 012102 (2001).
[8]V. Swamy, A. Kuznetsov, L. S. Dubrovinsky, R. A. Caruso, D. G. Shchukin, and B. C. Muddle, Phys. Rev. B **71**, 184302 (2005).
[9]G. Xiao, Y. Cao, G. Qi, L. Wang, C. Liu, Z. Ma, X. Yang, Y. Sui, W. Zheng, and B. Zou, J. Am. Chem. Soc. **139**, 10087 (2017).
[10]A. S. Kuznetsov, S. Sadofev, P. Schäfer, S. Kalusniak, and F. Henneberger, Appl. Phys. Lett. **105**, 191111 (2014).
[11]M. Wu, Y. Lu, and Y. Li, J. Am. Ceram. Soc. **90**, 3642 (2007).
[12]T. Nguyen, C. Dinh, and T. Do, ACS Nano **4**, 2263 (2010).
[13]S. Jiang, J. Liu, C. Lin, L. Bai, Y. Zhang, X. Li, Y. Li, L. Tang, and H. Wang, Solid State Commun. **169**, 37 (2013).
[14]L. Wang, Y. Pan, Y. Ding, W. Yang, W. L. Mao, S. V. Sinogeikin, Y. Meng, G. Shen, and H. Mao, Appl. Phys. Lett. **94**, 61921 (2009).
[15]S. Jiang, J. Liu, X. Li, L. Bai, W. Xiao, Y. Zhang, C. Lin, Y. Li, and L. Tang, J. Appl. Phys. **110**, 013526 (2011).
[16]H. R. Hoekstra, Inorg. Chem. **5**, 754 (1966).
[17]Q. Guo, Y. Zhao, C. Jiang, W. L. Mao, Z. Wang, J. Zhang, and Y. Wang, Inorg. Chem. **46**, 6164 (2007).
[18]Q. Guo, Y. Zhao, C. Jiang, W. L. Mao, and Z. Wang, Solid State Commun. **145**, 250 (2008).
[19]B. Wu, M. Zinkevich, F. Aldinger, D. Wen, and L. Chen, J. Solid State Chem. **180**, 3280 (2007).
[20]X. Ren, X. Yan, P. Wang, Y. Li, S. Wang, F. Peng, L. Xiong, J. Liu, and D. He, High Pressure Res. **34**, 70 (2014).
[21]K. A. Hoekstra and H. R. Gingerich, Science **146**, 1163 (1964).
[22]X. Ren, X. Yan, Z. Yu, W. Li, and L. Wang, J. Alloys Compd. **725**, 941 (2017).
[23]L. Wang, W. Yang, Y. Ding, Y. Ren, S. Xiao, B. Liu, S. V. Sinogeikin, Y. Meng, D. J. Gosztola, G. Shen, R. J. Hemley, W. L. Mao, and H. K. Mao, Phys. Rev. Lett. **105**, 095701 (2010).
[24]N. D. Sharma, J. Singh, S. Dogra, D. Varandani, H. K. Poswal, S. M. Sharma, and A. K. Bandyopadhyay, J. Raman Spectrosc. **42**, 438 (2011).
[25]P. M. Mao, H. K. Xu, and J. Bell, J. Geophys. Res. **91**, 4673, https://doi.org/10.1029/JB091iB05p04673 (1986).
[26]L. Zhang, S. Yan, S. Jiang, K. Yang, H. Wang *et al.*, Nucl. Sci. Tech. **26**, 060101 (2015).
[27]D. Hammersley, A. P. Svensson, S. O. Hanfland, M. Fitch, and A. N. Hausermann, High Pressure Res. **14**, 235 (1996).
[28]B. H. Toby, J. Appl. Crystallogr. **34**, 210 (2001).
[29]Y. He, J. F. Liu, W. Chen, Y. Wang, H. Wang, Y. W. Zeng, G. Q. Zhang, L. N. Wang, J. Liu, T. D. Hu, H. Hahn, H. Gleiter, and J. Z. Jiang, Phys. Rev. B **72**, 212102 (2005).
[30]Z. Yu, Q. Wang, Y. Ma, and L. Wang, J. Alloys Compd. **701**, 542 (2017).
[31]S. Jiang, J. Liu, C. Lin, X. Li, and Y. Li, J. Appl. Phys. **113**, 113502 (2013).
[32]F. X. Zhang, M. Lang, J. W. Wang, U. Becker, and R. C. Ewing, Phys. Rev. B **78**, 64114 (2008).
[33]X. Yang, Q. Li, Z. Liu, X. Bai, H. Song, M. Yao, B. Liu, and R. Liu, J. Phys. Chem. C **117**, 8503 (2013).
[34]F. D. Murnaghan, Proc. Nat. Acad. Sci. **30**, 244 (1944).
[35]F. Birch, Phys. Rev. **71**, 809 (1947).
[36]M. Zinkevich, Prog. Mater. Sci. **52**, 597 (2007).
[37]L. Xiong, J. Liu, L. Bai, Y. Li, C. Lin, D. He, F. Peng, and J. F. Lin, J. Appl. Phys. **113**, 033507 (2013).
[38]W. B. White and V. G. Keramidas, Spectrochim. Acta, Part A **28**, 501 (1972).
[39]J. Cui, G. A. Hope, J. Cui, and G. A. Hope, J. Spectrosc. **2015**, 1 (2015).
[40]D. Johnson, *ZView: A Software Program for IES Analysis, Version 2.8* (Scribner Associates Inc., Southern Pines, NC, 2002), p. 200.
[41]G. R. Hearne, J. Zhao, A. M. Dawe, V. Pischedda, M. Maaza, M. K. Nieuwoudt, P. Kibasomba, O. Nemraoui, J. D. Comins, and M. J. Witcomb, Phys. Rev. B **70**, 134102 (2004).
[42]V. Swamy, A. Kuznetsov, L. S. Dubrovinsky, P. F. Mcmillan, V. B. Prakapenka, G. Shen, and B. C. Muddle, Phys. Rev. Lett. **96**, 135702 (2006).
[43]Z. Quan, Y. Wang, I. Bae, W. Loc, C. Wang, Z. Wang, and J. Fang, Nano Lett. **11**(12), 5531 (2011).
[44]Q. Li, H. Zhang, R. Liu, B. Liu, D. Li, L. Zheng, J. Liu, T. Cui, and B. Liu, Nanoscale **8**, 2412 (2016).
[45]I. Halevy, R. Carmon, M. L. Winterrose, O. Yeheskel, and E. Tiferet, J. Phys.: Conf. Ser. **215**, 012003 (2010).